Effects of optical forces on the transmission of magnetic fluids investigated by *Z*-scan technique

Zi-Ming Meng,[1] Hai-Ying Liu,[1] Wei-Ren Zhao,[2] Wei Zhang,[2] Hai-Dong Deng,[1] Qiao-Feng Dai,[1] Li-Jun Wu,[1] Sheng Lan,[1,a)] and Achanta Venu Gopal[3]
[1]*Laboratory of Photonic Information Technology, School for Information and Optoelectronic Science and Engineering, South China Normal University, Guangzhou, Guangdong 510006, People's Republic of China*
[2]*School of Physics and Optoelectrics, Guangdong University of Technology, Guangzhou, Guangdong 510006, People's Republic of China*
[3]*Department of Condensed Matter Physics and Material Science, Tata Institute of Fundamental Research, Homi Bhabha Road, Mumbai 400005, India*

(Received 30 April 2009; accepted 11 July 2009; published online 21 August 2009)

The dependence of the transmission behavior of magnetic fluids on the incident power density of a laser beam is investigated and the conventional *Z*-scan technique is employed to continuously vary the optical forces induced by the laser beam. We calculate the optical forces exerted on magnetic nanoparticles and compare them with those for gold and silica nanoparticles. It is found that the optical forces for magnetic nanoparticles are comparable to those for gold nanoparticles. In addition, the calculation results show that the absorption force is dominant at low incident power densities while the gradient and scattering forces become significant at high incident power densities when the clustering of magnetic nanoparticles occurs. In *Z*-scan experiments, it is observed that the evolution of the *Z*-scan trace of a magnetic fluid with increasing incident power density cannot be explained only by the nonlinear absorption of the magnetic fluid induced by the thermal diffusion of magnetic nanoparticles. Instead, it indicates that the optical forces exerted on magnetic particles play an important role in determining the transmission of the magnetic fluid. This point is verified by comparing the *Z*-scan traces for magnetic fluids with different particle concentrations and carrier liquids. The effects of optical forces on the transmission of the magnetic fluids are also manifested in the morphology change of the magnetic fluids. © *2009 American Institute of Physics*. [DOI: 10.1063/1.3203938]

I. INTRODUCTION

Magnetic fluids or ferrofluids are liquids in which magnetic nanoparticles are uniformly distributed. They have attracted great interest in the fabrication of magneto-optical devices because of the formation of magnetic chains or columns in the presence of external magnetic fields which gives rise to many interesting phenomena such as birefringence, modulation of optical transmission, and magnetochromatics etc.[1–5] It is expected that these phenomena can be employed to realize some important magneto-optical devices such as optical switches, tunable gratings, and magnetic field sensors, etc.[6–12] In the past decade, much effort has been devoted to the study of the optical transmission through magnetic fluids. At the initial stage, the modification in the optical transmission of a magnetic fluid under an external magnetic field is attributed to the geometrical shadowing effect induced by the morphology change of the magnetic fluid, i.e., the formation of magnetic chains or clusters.[4,13,14] However, it was revealed recently by us that the geometrical shadowing effect cannot be responsible for the modification of optical transmission because the extinction ratios achieved by using an incandescent light and a laser light with the same power density are much different.[15] This phenomenon indicates clearly that the interaction between the laser beam and magnetic particles needs to be considered when the optical transmission of a magnetic fluid is concerned.

Now, it has been realized that the absorption and scattering of the incident light by magnetic particles or clusters may play an important role in determining the transmission of a magnetic fluid.[16] On the other hand, it is noticed that the modification in the optical transmission of a magnetic fluid can be induced only by the incident light itself, which is usually a laser beam, without applying an external magnetic field.[15,17,18] It has been shown that the laser-induced clustering of magnetic particles can significantly enhance the switching speed of the magnetic fluid under a magnetic flied.[15] An example that clearly shows the influence of the incident light on the transmission of magnetic fluids is the diffusion of magnetic particles driven by the thermal gradient which is induced by the absorption of the incident light by magnetic particles.[19–23] This phenomenon is referred to as the Soret effect and the resulting diffusion of magnetic particles may follow or against the direction of the thermal gradient, depending on the sign of the Soret coefficient. Thus, it is suggested that the optical transmission of a magnetic fluid may be modified by the dynamic migration of magnetic particles. Due to the existence of thermal diffusion, the refractive index and absorption of a magnetic fluid become dependent on the power density of the incident light. Conventional

a)Author to whom correspondence should be addressed. Electronic mail: slan@scnu.edu.cn.

Z-scan technique has been employed to characterize the nonlinear refractive index and absorption of magnetic fluids.[20,22,24]

In addition to the thermal diffusion mentioned above, however, dynamic migration of magnetic particles can also be induced by optical forces that have not been considered in previous literature. The purpose of this article is to demonstrate the effects of optical forces on the transmission of magnetic fluids. Similarly, the conventional *Z*-scan technique is employed in our studies. A physical picture is presented to describe the dynamic migration and clustering of magnetic particles induced by optical forces and their influences on optical transmission. The paper is organized as follows. In Sec. II, we calculate the optical forces exerted on magnetic particles and compare them with those for gold and silica particles. In Sec. III, we describe the magnetic fluid samples used in our study and the experimental setup. Then, the experimental results obtained in *Z*-scan processes for various samples are described and compared in Sec. IV. In Sec. V, we discuss the effects of optical forces and present a physical picture on how optical forces modify the optical transmission. Finally, a summary of our research work is given in Sec. VI.

II. OPTICAL FORCES EXERTED ON A MAGNETIC PARTICLE

As discussed above, it is thought that optical trapping plays a crucial role in determining the transmission of magnetic fluids through the induced dynamic migration and clustering of magnetic particles. Therefore, it is necessary to analyze the optical forces exerted on a magnetic particle, including gradient force, scattering force and absorption force. A comparison of these optical forces with those exerted on a metallic or a dielectric particle is also necessary and helpful for understanding the dynamic migration of magnetic particles induced by optical forces.

For a Rayleigh particle, the electrostatic approximation can be used to compute the polarizability which is given by[25]

$$\alpha = 3V\frac{\varepsilon - \varepsilon_m}{\varepsilon + 2\varepsilon_m}, \tag{1}$$

where $\varepsilon=\varepsilon_1+i\varepsilon_2$ and ε_m are the dielectric constants of the particle and the surrounding medium, and V is the volume of the particle. The maximum optical forces exerted on the particle are deduced to be[25]

$$F_g^{(m)} = \frac{I_0|\alpha|\sqrt{e}}{\varepsilon_m c r_0}, \tag{2a}$$

$$F_{\text{scat}}^{(m)} = \frac{8\pi^3 I_0|\alpha|^2\varepsilon_m}{3c\lambda^4}, \tag{2b}$$

$$F_{\text{abs}}^{(m)} = \frac{2\pi\varepsilon_m I_0\,\text{Im}(\alpha)}{\lambda c}. \tag{2c}$$

Here $F_g^{(m)}$, $F_{\text{scat}}^{(m)}$, and $F_{\text{abs}}^{(m)}$ stand for the maximum values of the gradient, scattering, and absorption forces exerted on the particle, I_0, r_0, and λ represent the intensity, radius and wavelength of the trapping light, respectively, and c is the speed of light in vacuum.

If we define an effective dielectric constant for the particle which is $\varepsilon_{\text{eff}}=\varepsilon-\varepsilon_m/\varepsilon+2\varepsilon_m$, then the real and imaginary parts as well as the module of the effective dielectric constant are derived to be

$$\text{Re}[\varepsilon_{\text{eff}}] = \frac{(\varepsilon_1-\varepsilon_m)(\varepsilon_1+2\varepsilon_m)+\varepsilon_2^2}{(\varepsilon_1+2\varepsilon_m)^2+\varepsilon_2^2}, \tag{3a}$$

$$\text{Im}[\varepsilon_{\text{eff}}] = \frac{3\varepsilon_m\varepsilon_2}{(\varepsilon_1+2\varepsilon_m)^2+\varepsilon_2^2}, \tag{3b}$$

$$|\varepsilon_{\text{eff}}| = \sqrt{\text{Re}[\varepsilon_{\text{eff}}]^2+\text{Im}[\varepsilon_{\text{eff}}]^2}. \tag{3c}$$

Hence, the three optical forces mentioned above can be expressed as

$$F_g^{(m)} = \frac{3I_0V|\varepsilon_{\text{eff}}|\sqrt{e}}{\varepsilon_m c r_0}, \tag{4a}$$

$$F_{\text{scat}}^{(m)} = \frac{24\pi^3 I_0V^2|\varepsilon_{\text{eff}}|^2\varepsilon_m}{c\lambda^4}, \tag{4b}$$

$$F_{\text{abs}}^{(m)} = \frac{6\pi\varepsilon_m I_0 V\,\text{Im}[\varepsilon_{\text{eff}}]}{\lambda c}. \tag{4c}$$

From Eqs. (4a)–(4c), it can be seen that the values of $F_g^{(m)}$ and $F_{\text{scat}}^{(m)}$ are determined by $|\varepsilon_{\text{eff}}|$ while that of $F_{\text{abs}}^{(m)}$ is governed by $\text{Im}[\varepsilon_{\text{eff}}]$. For particles made of different materials (i.e., different ε), the values of $|\varepsilon_{\text{eff}}|$ and $\text{Im}[\varepsilon_{\text{eff}}]$ can be much different. In order to compare the optical forces exerted on different particles, it is necessary to derive the relationship between $|\varepsilon_{\text{eff}}|$ (or $\text{Im}[\varepsilon_{\text{eff}}]$) and ε. In Figs. 1(a) and 1(b), we present the dependence of $|\varepsilon_{\text{eff}}|$ (or $\text{Im}[\varepsilon_{\text{eff}}]$) on ε in which the surrounding medium is assumed to be water (i.e., $n_m=1.33$ or $\varepsilon_m=1.7689$). We have marked in both figures the points corresponding to gold, magnetic, and silica particles. The dielectric constants for these three materials are found to be $-6.29+i2.04$, $4.8+i3.5$, and 2.1, respectively, for a trapping light at 0.532 μm.[26,27] It is remarkable that the values of $|\varepsilon_{\text{eff}}|$ and $\text{Im}[\varepsilon_{\text{eff}}]$ for magnetic particles are comparable to those for gold particles. They are much larger than those for silica particles.

In Table I, we present a comparison between different optical forces for gold, magnetic and silica nanoparticles. The radius of particles, the waist of the focus laser beam, and the intensity of the trapping light are chosen to be 0.006 μm, 5.0 μm, and 1.3×10^5 W/cm^2, respectively. These values are similar to those used in our experiments. In the calculation of the optical forces for gold and magnetic particles, we have used their effective volume, which is defined as

$$V' = 4\pi\int_0^a r^2\exp\left(\frac{r-a}{\delta}\right)dr,$$

instead of their real volume V. Here, δ is the skin depth.

From Table I, it can be seen that the maximum gradient force exerted on a gold particle is about four times of that

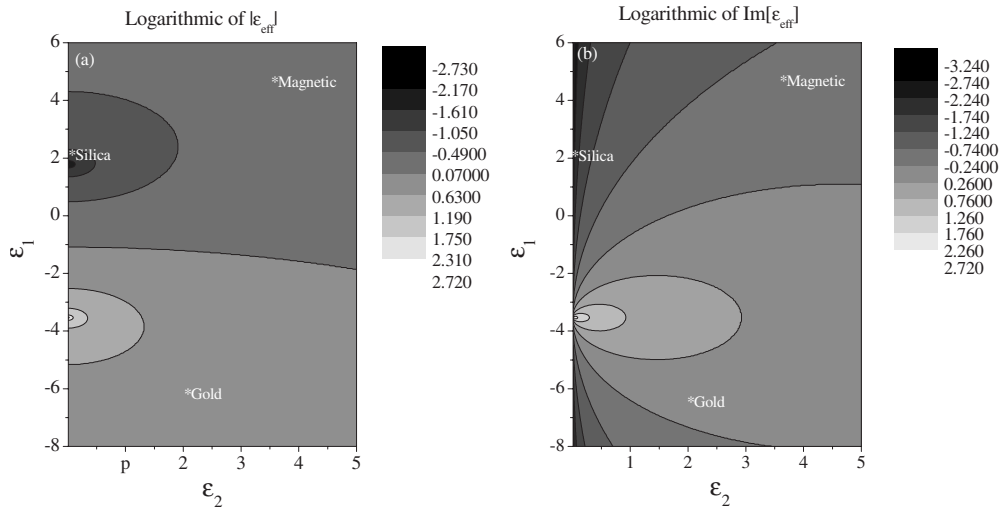

FIG. 1. (a) Dependence of the module of the effective dielectric constant ($|\varepsilon_{\text{eff}}|$) on the real and imaginary parts of the dielectric constant (ε_1 and ε_2). (b) Dependence of the imaginary part of the effective dielectric constant ($|\text{Im}[\varepsilon_{\text{eff}}]$) on the real and imaginary parts of the dielectric constant (ε_1 and ε_2). The points corresponding to magnetic, gold and silica particles are marked on the figures.

exerted on a magnetic particle. So is the absorption force. As for the scattering force, it is about twenty times of that exerted on a magnetic particle. The optical forces exerted on gold and magnetic particles are much larger than those exerted on silica particles. If we compare the optical forces for the same particles which are presented in Table II, it is found that for both gold and magnetic particles the absorption force is much larger than the gradient force while the scattering force is much smaller. For magnetic particles, the absorption force is fifty times of the gradient force while the scattering is only one percent of the gradient force. This result reminds us the important role of the absorption force in determining the transmission of magnetic fluids.

In Eq. (4), it is noticed that $F_g^{(m)}$ and $F_{\text{abs}}^{(m)}$ are proportional to V while $F_{\text{scat}}^{(m)}$ is proportional to V^2. In other words, $F_{\text{scat}}^{(m)}/F_g^{(m)}$ and $F_{\text{scat}}^{(m)}/F_{\text{abs}}^{(m)}$ increase in a rate of a^3 when the size of magnetic particles increases. This situation is shown in Fig. 2. Although $F_{\text{scat}}^{(m)}$ is quite small as compared with $F_g^{(m)}$ and $F_{\text{abs}}^{(m)}$ at the initial stage when the radius of magnetic particles is only ~6 nm, it increases rapidly and exceeds $F_g^{(m)}$ and $F_{\text{abs}}^{(m)}$ when the size of magnetic particles is enlarged to ~26 and ~95 nm, respectively. Therefore, the optical forces change significantly once the clustering of magnetic particles occurs. We can see later that this dramatic change in optical force plays a crucial role in determining the transmission behavior of magnetic fluids.

TABLE I. Comparison of various optical forces exerted on magnetic, gold and silica particles. The optical forces have been normalized with respect to $F_0=I_0r_0^2/c=1.1\times10^{-10}$ N. The parameters used in the calculation are $a=0.006$ μm, $r_0=5.0$ μm, $\lambda=0.532$ μm, $I_0=1.3\times10^5$ W/cm^2, and $V'=4\pi\int_0^a r^2\exp(r-a/\delta)dr$.

Type of particles	Dielectric constant ε	Optical forces in units of F_0		
		$F_g^{(m)}/F_0$	$F_{\text{scat}}^{(m)}/F_0$	$F_{\text{abs}}^{(m)}/F_0$
Magnet	$\varepsilon_1=4.8$, $\varepsilon_2=3.5$	1.023×10^{-8}	1.374×10^{-10}	5.084×10^{-7}
Gold	$\varepsilon_1=-6.29$, $\varepsilon_2=2.04$	4.698×10^{-8}	2.899×10^{-9}	2.001×10^{-6}
Silica	$\varepsilon_1=2.1$, $\varepsilon_2=0$	1.289×10^{-9}	2.184×10^{-12}	0

III. SAMPLE PREPARATION AND EXPERIMENTAL CONFIGURATION

The magnetic fluids used in our study were ester- and water-based Fe_3O_4 fabricated by the chemical coprecipitation technique. They were sealed into rectangular glass cells with a thickness of ~50 μm to form magnetic fluid films (MFFs). We prepared four samples which are labeled as E_1, E_2, W_1, and W_2 in the following for convenience. They stand for the ester-based MFF with a saturated magnetization of ~5 emu/g, the ester-based MFF with a saturated magnetization of ~1 emu/g, the water-based MFF with a volume fraction of ~7.9%, and the water-based MFF with a volume fraction of ~0.79%, respectively. It should be emphasized that the saturated magnetizations mentioned above are the values for the magnetic fluids (not for magnetic nanoparticles) and they depend on the volume fraction or concentration of magnetic nanoparticles in the magnetic fluids. In all samples, magnetic nanoparticles are not specially functionalized and their average diameter is ~12 nm. The viscosities of the pure ester and water are 600 and 1 mPa s, respectively. The experimental setup for an open-aperture Z-scan was employed to characterize the dependence of the transmission behavior of the MFFs on incident power density. The 532 nm laser beam from a solid-state laser was focused by a 5× objective lens onto the samples which were mounted on a translation stage. In this case, the radius of the laser beam is estimated to be ~5 μm at the focus point. A photodiode with a large surface (1×1 cm^2) was used to detect the transmitted light through the samples. The scanning speed was set

TABLE II. Comparison of various optical forces exerted on the same particles.

Type of particles	$F_{\text{scat}}^{(m)}/F_g^{(m)}$	$F_{\text{abs}}^{(m)}/F_g^{(m)}$
Magnet	1.343×10^{-2}	49.7
Gold	6.170×10^{-2}	42.6
Silica	1.694×10^{-3}	0

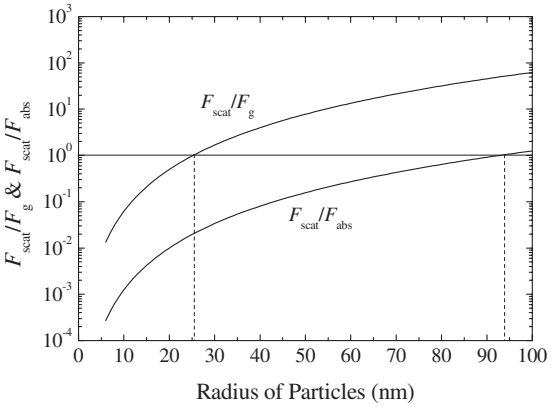

FIG. 2. Dependence of $F_{\mathrm{scat}}^{(m)}/F_g^{(m)}$ and $F_{\mathrm{scat}}^{(m)}/F_{\mathrm{abs}}^{(m)}$ on the radius of particles.

at 0.183 mm/s and the scanning region was chosen to be (−7.3, 7.3) mm. In order to improve the signal-to-noise ratio, a phase lock-in amplifier was used and the data acquisition system recorded the average value of every 200 data points with a sampling frequency of 1 kHz. We performed *Z*-scan experiments at different incident powers and the scanning process was repeated three times at each incident power. In *Z*-scan traces, the transmitted intensity is normalized with respect to the value at the starting point. In order to confirm the dynamic migration of magnetic particles induced by the incident laser beam, an inverted microscope (Zeiss Axio Observer A1) equipped with a charge coupled device (CCD) were used to monitor the morphology change of the MFFs. In this case, a 10× objective lens was used to focus the laser beam onto the samples and a halogen lamp was used for illumination.

IV. EXPERIMENTAL RESULTS

The influence of incident power density on the transmission of magnetic fluids was first observed in the switching operation of sample E_1 under an external magnetic field. The switching behaviors of sample E_1 under low and high incident power densities are compared in Figs. 3(a) and 3(b). In Fig. 3(a), it is noticed that the transmission of sample E_1 after the removal of the magnetic field increases gradually. Similar phenomenon has been reported by Li *et al.*[13,14] and it is ascribed to the increased remanence of the magnet after multiple switching operations which weakens the geometrical shadowing effect and results in a higher transmission. In sharp contrast, an opposite behavior is observed at high incident power densities, as shown in Fig. 3(b). The transmission after the withdrawal of the magnetic field decreases rapidly and the switching operation is severely deteriorated after several rounds. Apparently, this phenomenon implies that the incident power density has a great impact on the transmission behavior of magnetic fluids. However, the underlying physical mechanism remains unclear since it cannot be explained by the geometrical shadowing effect or the thermal diffusion model mentioned above.

Recently, it was found by us that the clustering of magnetic particles appears at a moderate incident power density and it results in a significant enhancement in the switching speed of MFFs.[15] This phenomenon indicates clearly the existence of optical forces exerted on magnetic particles. Thus, it is believed that the optical transmission of MFFs will be affected by optical forces in the form of migration and/or clustering of magnetic particles. In fact, it has been shown that clustering or assembling of polymer and gold nanoparticles can be induced by a focused laser beam. Yoshikawa and co-workers[28] and Hosokawa *et al.*[29] studied the cluster formation by polystyrene latex nanoparticles and suggested that optical trapping, escape of particles, and clustering of particles dynamically codetermine the assembly process. In addition, reversible assembly of gold nanoparticles was also demonstrated.[30]

The *Z*-scan traces for sample E_1 at low and high incident powers are shown in Figs. 4(a) and 4(b), respectively. A transmission peak is observed at the focus point for an incident power density as low as 3×10^3 W/cm^2 (or an incident power of 3 mW in our case). The radius of the laser beam at the focus point is estimated to be ~5 μm. With increasing incident power, the *Z*-scan trace remains nearly unchanged. However, the transmission peak appearing at the focus point is replaced by a transmission valley when the incident power reaches 20 mW. Now obvious difference in the *Z*-scan trace is found for different scanning processes. The *Z*-scan trace with a transmission valley at the focus point is maintained till an incident power as high as 100 mW. However, the *Z*-scan trace is found to degrade for incident powers higher than 50 mW. In the terminology of nonlinear optics, the evolution of the open-aperture *Z*-scan trace for sample E_1 indicates a change in the sign of nonlinear absorption coefficient

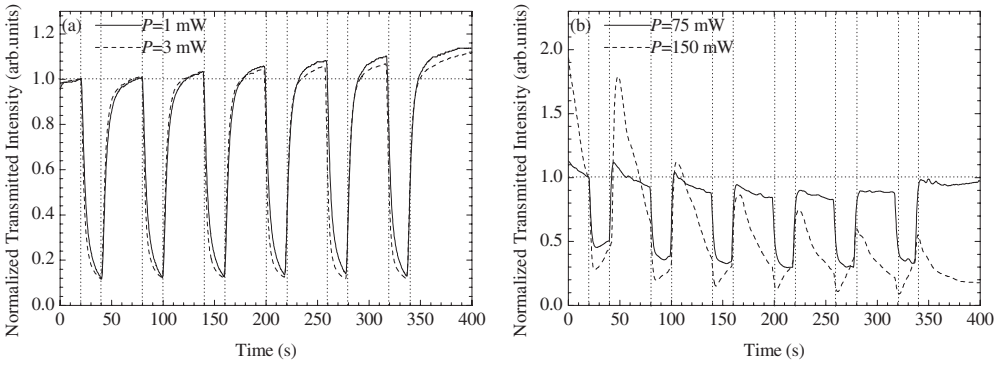

FIG. 3. Influence of incident power density on the transmission of magnetic fluids observed in the switching operations under (a) low and (b) high power densities.

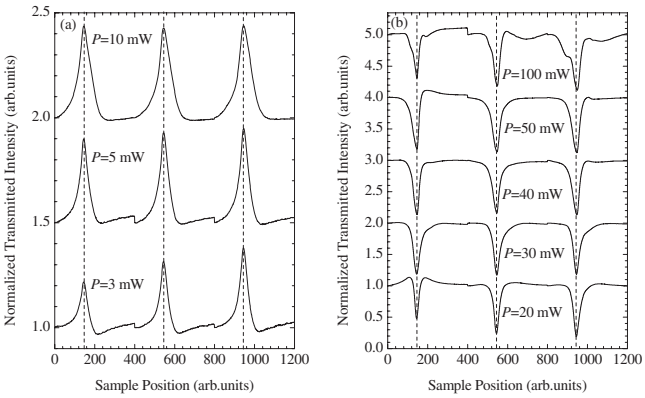

FIG. 4. *Z*-scan traces for sample E_1 obtained at different incident powers. The radius of the laser beam at the focus point is estimated to be 5 μm. (a) Three consecutive *Z*-scan traces obtained at low incident powers of 3, 5, and 10 mW. (b) Three consecutive *Z*-scan traces obtained at high incident powers of 20, 30, 40, 50, and 100 mW.

with increasing incident power density. However, a careful examination of the *Z*-scan traces reveals several remarkable features which can be identified in Fig. 5. First, asymmetric profiles are observed at all incident powers. Second, the transmission change at the focus point is quite large. For example, the transmission drops to ~17% at an incident power of 30 mW. Finally, the transmission peaks observed at low incident powers are replaced by the transmission valleys at high incident powers. All these features indicate that the transmission peaks or valleys do not originate from the nonlinear absorption of the magnetic fluid. This issue will be addressed in detail in Sec. V.

The dependence of the *Z*-scan trace on the incident power for sample E_2 with a lower concentration of magnetic particles is presented in Fig. 6. As compared with sample E_1, the *Z*-scan trace for sample E_2 and its evolution with increasing incident power appear to be more complicated. For incident powers lower than 10 mW, we can see a shallow and wide transmission valley in which a tiny transmission peak is observed in each *Z*-scan trace. When the incident power reaches 10 mW, the tiny transmission peak evolves into a sharp and narrow one seating on the valley. As the incident power is further raised to 20 mW, the transmission valley disappears and an asymmetric transmission peak appears. However, a regular transmission valley similar to that observed in sample E_1 does not appear even at an incident power of 40 mW. Instead, we observe a relatively strange *Z*-scan trace and it appears to be different in different scanning processes. Anyway, it is still possible to recognize a drop in the saddlelike profile at 50 mW. The general trend observed in the power dependence of the *Z*-scan for sample E_2 is similar to that observed in sample E_1, i.e., a transmission peak is found at low incident powers and it evolves into a transmission valley at high incident powers.

As compared with ester, water has a much smaller viscosity. Thus, it is expected that the response of magnetic nanoparticles to the irradiation of laser beam in water-based samples should be much faster. The *Z*-scan traces for sample W_1 measured at different incident powers are shown in Fig. 7. It can be seen that a transmission valley appears at a lower incident power of 20 mW. A further increase in incident power leads to the degradation of the *Z*-scan trace. At an incident power of 100 mW, the *Z*-scan trace is severely distorted, indicating an active migration of magnetic particles. As for sample W_2, no characteristic peaks or valleys are observed even for an incident power as large as 100 mW. In addition, the normalized transmission at the focus point is much smaller as compared to those observed in other samples. Therefore, it is concluded that the dilution significantly weakens the response of magnetic nanoparticles to the incident laser beam.

In principle, the dynamic migration or clustering of magnetic particles should be manifested in the morphology change of the magnetic fluids. Thus, we have used the CCD attached on the microscope to monitor and record the morphology change of the samples under the illumination of the incident laser beam. Basically, the power density of the incident light can be adjusted either by varying the beam size or by changing the laser power. In *Z*-scan experiments, we chose the former to vary incident power density. Now we fix the beam size and change the incident power. A comparison of the morphology changes observed in different samples is presented in Fig. 8. In Figs. 8(a) and 8(b), we show the morphology change in samples E_1 induced by increasing incident power. At low incident powers, we can see a bright spot at the beam center which indicates a lower concentration of magnetic particles, as shown in Fig. 8(a). This situation corresponds to the appearance of the transmission peaks observed in *Z*-scan traces. At high incident powers, however, a large number of clusters appear at the beam center, as

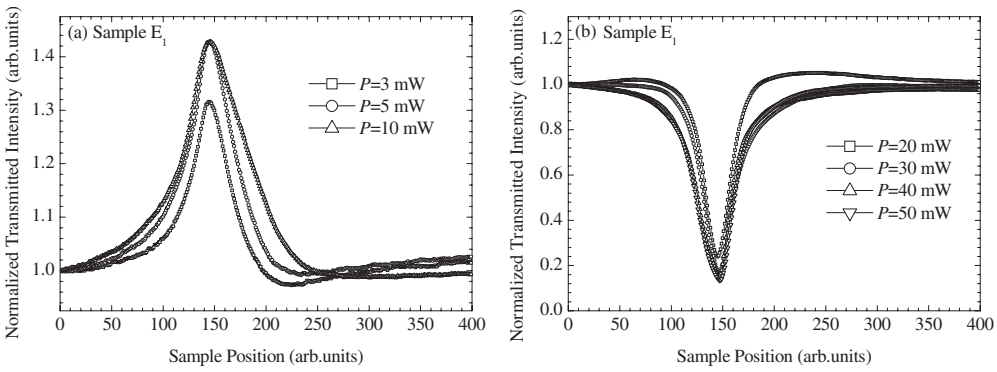

FIG. 5. Comparison of the *Z*-scan traces for sample E_1 obtained at (a) low and (b) high incident powers.

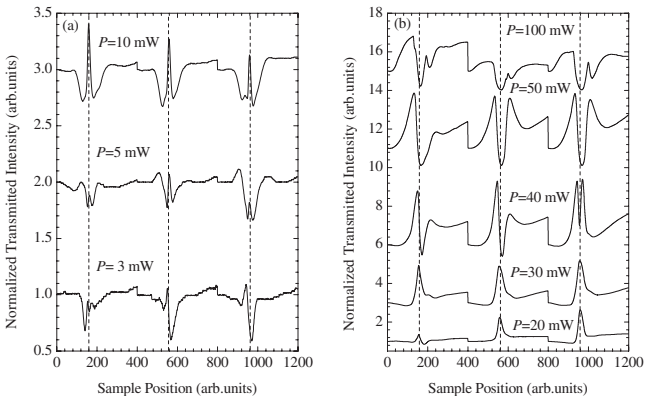

FIG. 6. *Z*-scan traces for sample E_2 obtained at different incident powers. The radius of the laser beam at the focus point is estimated to be 5 μm. (a) Three consecutive *Z*-scan traces obtained at low incident powers of 3, 5, and 10 mW. (b) Three consecutive *Z*-scan traces obtained at high incident powers of 20, 30, 40, 50, and 100 mW.

evidenced in Fig. 8(b). It is responsible for the transmission valleys found in *Z*-scan traces. Some small grains are observed in the images shown in Figs. 8(a) and 8(b) and they are caused by two reasons. One is that the dispersion of magnetic nanoparticles in the ester is not as good as that in water. The other is the clusters formed at high power densities do not completely disperse into nanoparticles after removing the laser light. As compared with the ester-based samples, the response of the water-based samples appears to be much faster. Once the laser beam is turned on, the clustering of magnetic nanoparticles occurs quickly and the beam region becomes dark, as shown in Fig. 8(c) for sample W_1 at an incident power of 30 mW. This is associated with the transmission valleys observed in the *Z*-scan traces. Figure 8(d) shows the situation when the incident power is raised to 50 mW. We can see a bright region at the beam center which is associated with the transmission peaks in the *Z*-scan traces. For sample W_2, no obvious change is found at 100 mW, as shown in Fig. 8(e). However, clustering or assembling of magnetic particles occurs when the incident power is increased to 300 mW, as shown in Fig. 8(f). This observation is in good agreement with that observed in the *Z*-scan experiments. The dynamic migration and clustering of magnetic particles and the resulting morphology change are closely related to the optical forces exerted on magnetic particles. A physical picture describing the response of magnetic particles to the incident laser beam will be presented in Sec. V.

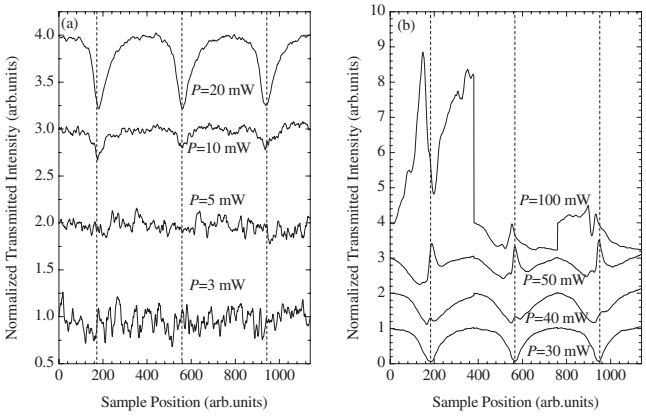

FIG. 7. *Z*-scan traces for sample W_1 obtained at different incident powers. The radius of the laser beam at the focus point is estimated to be 5 μm. (a) Three consecutive *Z*-scan traces obtained at low incident powers of 3, 5, 10, and 20 mW. (b) Three consecutive *Z*-scan traces obtained at high incident powers of 30, 40, 50, and 100 mW.

V. PHYSICAL MODEL FOR DYNAMIC MIGRATION AND CLUSTERING OF MAGNETIC NANOPARTICLES

In Sec. IV, we have mentioned that three remarkable features can be identified in the *Z*-scan traces of sample E_1, as shown in Fig. 5. We think that the transmission peaks or valleys cannot be attributed to the nonlinear absorption of magnetic fluids because of the following reasons. First, it is well known that the expression for the nonlinear absorption in the *Z*-scan theory takes the form[24]

$$T(z,t) = \frac{\ln[1 + q_0(z,t)]}{q_0(z,t)}, \tag{5a}$$

$$q_0(z,t) = \frac{\beta I_0(t) L_{\text{eff}}}{1 + \left(\frac{z}{Z_R}\right)^2}. \tag{5b}$$

Here, $I_0(t)$, L_{eff}, Z_R, and β represent the on-axis intensity at the focus, the effective sample length, the Rayleigh length, and the two-photon absorption coefficient, respectively. It is found, however, that the transmission profiles observed in the *Z*-scan experiments cannot be described by the analytical expression for the nonlinear absorption given in Eq. (5). The observed asymmetric profiles severely deviate from the symmetric one described by Eq. (5). In addition, the large transmission contrast achieved at the focal point requires an unrealistic large value of β because the maximum incident

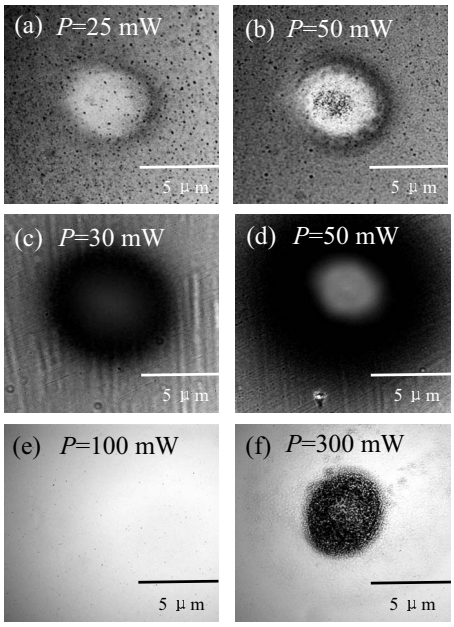

FIG. 8. Morphology changes of different magnetic fluids induced by increasing incident power. The radius of the laser beam is estimated to be 5 μm. (a) Sample E_1 at 25 mW; (b) sample E_1 at 50 mW; (c) sample W_1 at 30 mW; (d) sample W_1 at 50 mW; (e) sample W_2 at 100 mW; and (f) sample W_2 at 300 mW.

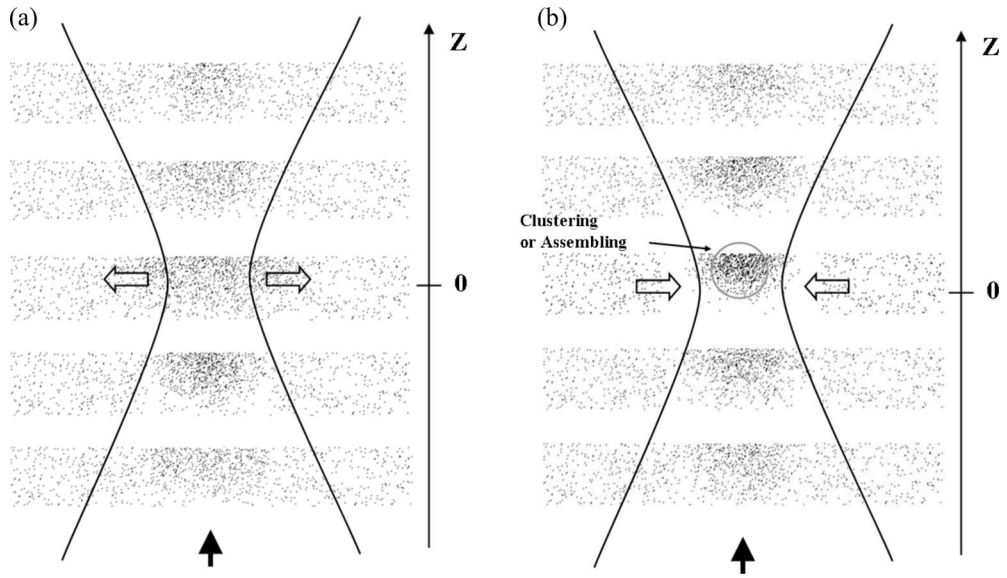

FIG. 9. Schematic showing the dynamical migration and clustering of magnetic particles induced by optical forces in the *Z*-scan processes under (a) low and (b) high incident powers.

power intensity used in the experiments is only 100 kW/cm^2. Therefore, it is concluded that the transmission profiles observed in the *Z*-scan experiments cannot be explained by the nonlinear absorption of magnetic fluids.

Based on the Lambert–Beer law, the optical transmission through a sample is directly related to the extinction coefficient of the sample. In the Rayleigh scattering regime where particles are much smaller than the wavelength of the incident light, the extinction coefficient originates from the absorption and scattering of the incident light by magnetic nanoparticles. However, it is too complicated to analytically describe the influence of the dynamic migration of a large number of magnetic particles driven by optical forces on the optical transmission of magnetic fluids. After a careful inspection of all experimental observations, we have generalized a physical picture which can qualitatively describe the effects of optical forces on the transmission of magnetic fluids and reasonably explained the experimental observations. The dynamic migration and clustering of magnetic particles based on this model are schematically shown in Figs. 9(a) and 9(b) for low and high incident powers, respectively.

It has been shown that the clustering or assembling of nanoparticles induced by optical trapping is a dynamic process which can be described as the cooperation of optical trapping, escape, and clustering.[28] The optical trapping is induced by the gradient force of the focused laser beam which tends to drive particles into the beam region.[31–34] The escape process is described as the movement of particles out of the beam region which is directly related to the Brownian motion. Specifically, the effects of the scattering and absorption forces are also included in this process. Clustering of particles is induced by optical trapping. When we examine the transmission behavior of samples E_1, E_2, and W_1, it is found that the *Z*-scan traces for these three samples appear to be different at low incident powers. At high incident powers when the gradient force becomes dominant, they exhibit similar profiles with a transmission valley observed at the focus point. Therefore, it is necessary to interpret the underlying physical mechanism that leads to the difference found at low incident powers.

As mentioned above, the two major mechanisms that result in dynamic migration of nanoparticles are thermal diffusion and optical force. It is thought that the former mechanism is dominant when the optical forces are not strong at low incident powers. Once the optical forces become effective, the transmission of the magnetic fluids is determined by the competition of these two mechanisms. In thermal diffusion, the direction of particle migration depends on the sign of the Soret coefficient. Particles migrate along and against the thermal gradient for a positive and a negative Soret coefficient, respectively. For a positive Soret coefficient, the movement of magnetic particles out of the illumination region will leads to a reduction in the thermal gradient which alleviates the thermal diffusion.[19,23] In case of a negative Soret coefficient, the accumulation of magnetic particles induced by the thermal diffusion in the beam region creates a gradient in the concentration of particles which prohibits the further diffusion of particles. At low incident powers, the cooperation of the absorption force and Brownian motion dominates the movement of magnetic particles and the escape process is pronounced. The magnetic nanoparticles within the beam volume are pushed forward, resulting in a higher concentration in the front part of the sample. This gradient in the concentration of particles will induce a diffusion of nanoparticles out of the beam volume because the gradient force in the transverse direction is too weak to provide a confinement for particles. This situation is schematically depicted in Fig. 9(a). This kind of diffusion, which is caused mainly by the absorption force in the forward direction, results in a lower particle concentration at the beam center and a transmission peak in the *Z*-scan trace. Therefore, the absorption force tends to push magnetic particles out of the beam region at low incident powers. On the other hand, the thermal diffusion will drive magnetic particles in or out

of the beam region, depending on the sign of the Soret coefficient. In sample E_2, we observe a slight decrease in transmission when the sample is moved toward the focus point. It implies that magnetic particles in the ester-based samples possess a negative Soret coefficient. Therefore, the transmission behavior of magnetic fluids is eventually determined by the competition between the thermal diffusion and the absorption force. In sample E_1 with a high particle concentration, the escape of magnetic particles out of the beam region is dominant. As a result, only a transmission peak is observed at the focus point. As for sample E_2 with a low particle concentration, the situation is different. At low incident powers, a reduction of transmission is observed when the sample is far away from the focus point. In this case, we think that the migration of magnetic particles toward the beam center due to thermal diffusion is dominant. Near the focus point, the absorption force becomes quite strong and the movement of magnetic particles becomes dominated by the escape out of the beam region. Consequently, a tiny transmission peak appears at the focus point and it evolves into a sharp one with increasing incident power. In sample W_1, it is thought that the migration of magnetic particles toward the beam region induced by the thermal diffusion is counteracted by the escape of magnetic particles out of the beam region caused by the absorption force at low incident powers (3 and 5 mW). Hence, no obvious transmission peak or valley is observed in *Z*-scan traces.

With increasing incident power, the gradient force in the transverse direction becomes stronger and the optical trapping becomes significant. However, a stable trapping requires that the trapping potential must be larger than the thermal kinetic energy. Since the gradient force is proportional to the volume of particles, it is expected that the clustering of particles induced by optical trapping will in turn significantly enhance the trapping force. In our case, the well-dispersed magnetic nanoparticles with an average diameter of ~12 nm are difficult to be stably trapped by using an objective lens with a small numerical aperture (NA=0.1 in our case) unless the clustering of particles is induced. The optical trapping potential can be expressed as[30]

$$U = -\frac{|\alpha||E|^2}{2} = -\frac{I}{c}3V\left|\frac{(n/n_m)^2-1}{(n/n_m)^2+2}\right|, \tag{6}$$

where α stands for the polarizability and V is the volume of the trapped particle, n and n_m represent the refractive indices of the particle and surrounding medium, respectively. In the extreme case when

$$\lim_{(n/n_m)^2\to\infty}\left[\left|\frac{(n/n_m)^2-1}{(n/n_m)^2+2}\right|\right] = 1,$$

the maximum trapping potential is estimated to be $\sim -36 \times 10^{-6}$ eV at an incident power of ~100 mW. This value is much smaller than the thermal kinetic energy at room temperature which is $\sim 26\times 10^{-3}$ eV. Once the clustering of magnetic nanoparticles occurs, however, the trapping potential is greatly enhanced due to the enlarged volume of the trapped clusters. For example, if magnetic particles aggregate into magnetic clusters of ~120 nm in diameter, the maximum trapping potential will become -36×10^{-3} eV which is enhanced by three orders of magnitude. In this case, a stable optical trapping can be achieved. Once the trapped particles become even larger, however, the scattering force will exceed the gradient force and the particles will be pushed out of the beam volume. This is because $F_{\text{scat}}^{(m)}/F_g^{(m)} \propto F_{\text{scat}}^{(m)}/F_{\text{abs}}^{(m)} \propto a^3$, as can be seen in Fig. 2. As a result, a transmission peak appears in the *Z*-scan trace. The situation like this is observed in sample W_1 when the incident power is increased to 50 mW.

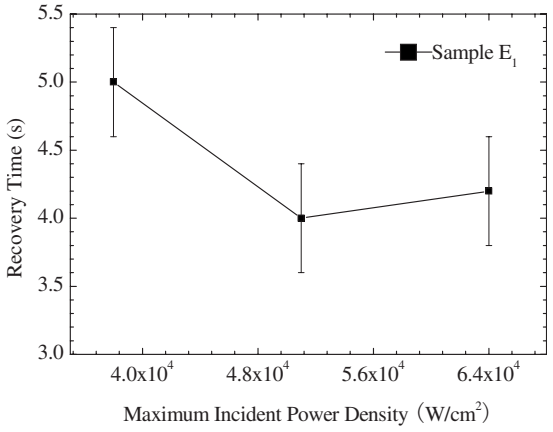

FIG. 10. Dependence of the recovery time on incident power density observed in the *Z*-scan processes for sample E_1.

At high incident powers, the increase in the gradient force tends to attract and confine magnetic particles in the beam volume, leading to a decreased transmission at the focus point. More importantly, the formed magnetic clusters with a larger volume will result in a much stronger scattering of the incident light, leading to a dramatic reduction in the transmission of the magnetic fluid. This situation is schematically illustrated in Fig. 9(b). Due to the small viscosity of water, the transition from the dynamic migration to the clustering occurs at a lower threshold for the water-based samples as compared with the ester-based ones.

It should be emphasized that the thermal diffusion also contributes to the dynamic migration and clustering of nanoparticles in the *Z*-scan processes. Since the transition from a transmission peak to a transmission valley can only be explained by taking the optical forces into account, it is thought that the thermal diffusion of magnetic particles does not play a dominant role in determining the optical transmission of magnetic fluids. In addition, we have analyzed the recovery times derived from the *Z*-scan traces for sample E_1 and the results for incident powers of 30, 40, and 50 mW are compared in Fig. 10. If the transmission peaks or valleys originated from the thermal diffusion of magnetic particles, then the recovery time would reflect the disappearance of the thermal gradient and it would increase with increasing incident power. However, the recovery time does not exhibit any dependence on the incident power. Therefore, we think that optical forces do play a dominant role in determining the optical transmission of magnetic fluids.

VI. CONCLUSION

In summary, we have employed the conventional *Z*-scan technique to investigate the effects of optical forces on the

optical transmission of magnetic fluids. It is found that the transmission peaks or valleys observed in the *Z*-scan traces cannot be explained by the nonlinear absorption of magnetic fluids induced by the thermal diffusion of magnetic particles. We have established a physical model based on the dynamic migration and clustering of magnetic particles induced by optical forces. It is revealed that the dynamic migration of magnetic particles is governed by the absorption force at low power densities while the clustering of magnetic particles induced by the gradient force become dominant at high power densities. Our finding is helpful not only for understanding the transmission behavior of magnetic fluids but also for manipulating magnetic particles.

ACKNOWLEDGMENTS

The authors acknowledge the financial support from the National Natural Science Foundation of China (Grant Nos. 10674051 and 10811120010) and the Program for Innovative Research Team of the Higher Education in Guangdong (Grant No. 06CXTD005).

[1]N. A. Yusuf, H. A. Safia, and I. A. Aljarayesh, J. Appl. Phys. **73**, 6136 (1993).
[2]Z. Y. Di, X. F. Chen, S. L. Pu, X. Hu, and Y. X. Xia, Appl. Phys. Lett. **89**, 211106 (2006).
[3]J. E. Martin, K. M. Hill, and C. P. Tigges, Phys. Rev. E **59**, 5676 (1999).
[4]S. Y. Yang, Y. P. Chiu, B. Y. Jeang, H. E. Horng, C. Y. Hong, and H. C. Yang, Appl. Phys. Lett. **79**, 2372 (2001).
[5]S. Y. Yang, J. J. Chieh, H. E. Horng, C. Y. Hong, and H. C. Yang, Appl. Phys. Lett. **84**, 5204 (2004).
[6]H. E. Horng, C. Y. Hong, W. B. Yeung, and H. C. Yang, Appl. Opt. **37**, 2674 (1998).
[7]J. W. Seo, S. J. Park, and K. O. Jang, J. Appl. Phys. **85**, 5956 (1999).
[8]H. E. Horng, C. S. Chen, K. L. Fang, S. Y. Yang, J. J. Chieh, C. Y. Hong, and H. C. Yang, Appl. Phys. Lett. **85**, 5592 (2004).
[9]H. E. Horng, C. Y. Hong, S. L. Lee, C. H. Ho, S. Y. Yang, and H. C. Yang, J. Appl. Phys. **88**, 5904 (2000).
[10]H. E. Horng, S. Y. Yang, S. L. Lee, C. Y. Hong, and H. C. Yang, Appl. Phys. Lett. **79**, 350 (2001).
[11]J. Monin, O. B. Philibert, V. Cabuil, and L. Delaunay, Proc. SPIE **1274**, 316 (1990).
[12]G. V. Kurlyandskaya, M. L. Sánchez, B. Hernando, V. M. Prida, P. Gorria, and M. Tejedor, Appl. Phys. Lett. **82**, 3053 (2003).
[13]J. Li, B. G. Zhao, Y. Q. Lin, X. Y. Qiu, and X. J. Ma, J. Appl. Phys. **92**, 1128 (2002).
[14]J. Li, X. D. Liu, Y. Q. Lin, L. Bai, Q. Li, X. M. Chen, and A. R. Wang, Appl. Phys. Lett. **91**, 253108 (2007).
[15]H. D. Deng, J. Liu, W. R. Zhao, W. Zhang, X. S. Lin, T. Sun, Q. F. Dai, L. J. Wu, S. Lan, and A. V. Gopal, Appl. Phys. Lett. **92**, 233103 (2008).
[16]J. Philip, J. M. Laskar, and B. Raj, Appl. Phys. Lett. **92**, 221911 (2008).
[17]B. Hoffmann and W. Köhler, J. Magn. Magn. Mater. **262**, 289 (2003).
[18]R. R. Kellner and W. Köhler, J. Appl. Phys. **97**, 034910 (2005).
[19]N. V. Tabiryan and W. L. Luo, Phys. Rev. E **57**, 4431 (1998).
[20]S. Alves, G. Demouchy, A. Bee, D. Talbot, A. Bourdon, and A. M. Figueiredo Neto, Philos. Mag. **83**, 2059 (2003).
[21]P. Kopčanský, M. Hnatič, M. Repašan, I. Potočová, M. Timko, I. Turek, J. Štelina, C. Musil, J. Braciník, E. Ayrjan, L. Vekas, and D. Bica, J. Magn. Magn. Mater. **289**, 292 (2005).
[22]S. Alves, F. L. Sant'Anna Cuppo, A. Bourdon, and A. M. Figueiredo Neto, J. Opt. Soc. Am. B **23**, 2328 (2006).
[23]T. D. Du and W. L. Luo, J. Appl. Phys. **85**, 5953 (1999).
[24]M. Sheik-Bahae, A. A. Said, T. H. Wei, D. J. Hagan, and E. W. Van Stryland, IEEE J. Quantum Electron. **26**, 760 (1990).
[25]K. Svoboda and S. M. Block, Opt. Lett. **19**, 930 (1994).
[26]E. D. Palik, *Handbook of Optical Constant of Solids* (Academic, Orlando, 1985).
[27]A. Schlegel, S. F. Alvarado, and P. Wachter, J. Phys. C **12**, 1157 (1979). (Fe_3O_4)
[28]C. Hosokawa, H. Yoshikawa, and H. Masuhara, Phys. Rev. E **70**, 061410 (2004).
[29]C. Hosokawa, H. Yoshikawa, and H. Masuhara, Phys. Rev. E **72**, 021408 (2005).
[30]H. Yoshikawa, T. Matsui, and H. Masuhara, Phys. Rev. E **70**, 061406 (2004).
[31]A. Ashkin, J. M. Dziedzic, J. E. Bjorkholm, and S. Chu, Opt. Lett. **11**, 288 (1986).
[32]Y. Zhang, C. Gu, A. M. Schwartzberg, S. W. Chen, and J. Z. Zhang, Phys. Rev. B **73**, 165405 (2006).
[33]J. Liu, Q. F. Dai, Z. M. Meng, X. G. Huang, L. J. Wu, Q. Guo, W. Hu, S. Lan, A. V. Gopal, and V. A. Trofimov, Appl. Phys. Lett. **92**, 233108 (2008).
[34]Q. F. Dai, H. Y. Liu, J. Liu, L. J. Wu, Q. Guo, W. Hu, X. B. Yang, S. H. Liu, S. Lan, A. V. Gopal, and V. A. Trofimov, Appl. Phys. Lett. **92**, 153111 (2008).